


 Cite this: *RSC Adv.*, 2024, **14**, 12853

The influence of hydrogen bonding on the structure of organic–inorganic hybrid catalysts and its application in the solvent-free epoxidation of α -olefins[†]

 Hong-Bin Ju,^{‡abde} Li-Zhi Zhang,^{‡ce} De-Bao Li,^{*a} Tao Geng,^{ID *be} Ya-Jie Jiang^{be} and Ya-Kui Wang^{be}

In this study, two types of catalysts were prepared by the combination of gemini quaternary ammonium salt with two distinct species of phosphotungstic acid. Catalysts prepared by the Wells–Dawson type of phosphotungstic acid and Keggin-type phosphotungstic acid both exhibited dual-phase catalytic behavior, demonstrating both heterogeneous and homogeneous catalytic activities. In comparison to the catalyst prepared by the Keggin-type phosphotungstic acid, due to the higher size of Wells–Dawson type of phosphotungstic acid, hydrogen bonding could not effectively affect the catalyst prepared by $H_6P_2W_{18}O_{62}$. Subsequently, the influential factors on the catalytic reaction were investigated. Through the utilization of techniques such as XPS, FT-IR, Raman spectra and other characterization methods, two distinct structure and reaction mechanisms for these catalysts were elucidated under the influence of hydrogen bonding.

 Received 23rd February 2024
 Accepted 3rd April 2024

 DOI: 10.1039/d4ra01399a
rsc.li/rsc-advances

1. Introduction

Epoxides represent crucial raw materials for the synthesis of fine chemicals, finding extensive applications in nanomaterials, surfactants, food additives, and cosmetics.^{1,2} Industrially, olefin epoxidation has consistently remained the primary method for producing epoxides. The 1,2-epoxy alkanes synthesized by α -olefins serve as specific intermediates for synthesizing high-value chemicals,^{3,4} presenting a distinct application potential, particularly in the realm of surfactants.^{5,6}

In the context of olefin epoxidation, catalysts have played a pivotal role.^{7,8} Broadly, these catalysts can be categorized as either metal-based or inorganic catalysts.^{9,10} Among metal-based catalysts, transition metal-based catalysts have garnered extensive attention owing to their efficient atomic utilization of oxidants.¹¹ Typically, these catalysts are prepared into metal-organic frameworks,⁶ polymers,^{12,13} phase-transfer catalysts

(PTCs),¹⁴ and microemulsions¹⁵ to enhance their catalytic efficiency. The majority of these catalysts are heterogeneous in nature, they may pose certain risks due to the rigorous reaction conditions required for achieving high yields.¹⁶ Furthermore, the limited solubility of certain types of homogeneous catalysts under catalytic conditions, along with challenges in separation processes, present significant hurdles for researchers.¹⁷

As a kind of widely used phase-transfer catalysts (PTCs), Ishii–Venturello catalysts¹⁸ have gained widespread use in epoxidation, owing to their mild catalytic conditions and recyclable characteristics.¹⁹ Prepared by heteropoly acid and ammonium salt,²⁰ these catalysts offer a blend of advantages associated with both heterogeneous and homogeneous catalysts. However, the addition of solvents in the catalytic process for catalyst protection contradicts the principles of green chemistry.^{21,22} Catalysts developed for olefin epoxidation under solvent-free conditions were generally only used to oxidize cycloolefins²³ or require more stringent reaction conditions.²⁴ Consequently, the present research goals lie in enabling catalysts to function without the addition of solvents.

PTCs prepared by polyoxometalates and Gemini quaternary ammonium salts exhibited an enhanced ability to penetrate the oil–water interface to the oil phase under solvent-free conditions. Not only did they demonstrate exceptional catalytic performance, but also facilitated easier recovery from the reaction system.^{25,26} Among these catalysts, the utilization of Keggin-type polyoxometalates (POMs) was prevalent due to their outstanding oxidation catalytic performance.^{27,28} In theory, by

^aInstitute of Coal Chemistry, Chinese Academy of Sciences, Taiyuan 030001, Shanxi, China. E-mail: dbli@sxic.ac.cn

^bChina Research Institute of Daily Chemistry Co., Ltd, Taiyuan 030001, Shanxi, China. E-mail: anhuanjianjishi@163.com

^cChina Research Institute of Daily Chemical Industry, Taiyuan 030001, Shanxi, China

^dUniversity of Chinese Academy of Sciences, Beijing 100049, China

^eShanxi Key Laboratory of Functional Surfactants, Taiyuan 030001, Shanxi, China

[†] Electronic supplementary information (ESI) available. See DOI: <https://doi.org/10.1039/d4ra01399a>

[‡] These authors contributed to the work equally and should be regarded as co-first authors.



the formation of hydrogen bonds in POM, on the one hand, suggesting strong host-guest interactions in two substances could be enhanced,²⁹ on the other hand, such strong interactions tightened interface contact and accelerated interface electron transfer of catalyst,³⁰ making the catalytic performance more effective. Wells-Dawson-type phosphotungstic acid, characterized by its nanoscale dimensions of approximately 1 nm, can be viewed as an enhanced Keggin-type cluster, offering a greater number of organic ligands.^{31,32} Additionally, it provides more redox active sites. Despite these advantages, this species has not been as extensively employed in epoxidation reactions.^{33,34}

In this study, two different types of organic-inorganic composite catalyst was prepared, incorporating Wells-Dawson-type phosphotungstic acid and Keggin-type phosphotungstic acid in combination with a gemini quaternary ammonium salt. Compared with our previous study,³⁵ due to the addition of hydroxyl groups in the quaternary ammonium salt, the new catalyst prepared by Keggin-type phosphotungstic acid showed distinct microstructure and reaction mechanism. Subsequently, a comparative analysis was performed between catalysts prepared by Keggin type and Wells-Dawson type phosphotungstic acid, leading to the deduction of distinct reaction mechanisms underlying these catalysts.

2. Material and methods

2.1 Materials

1,3-Dichloro-2-propanol, propanol, sodium carbonate, 1-dodecene, 1-octene, 1-tetradecene, 1-hexadecene, hydrogen peroxide, phosphotungstic acid, phosphoric acid ethyl alcohol, and methyl alcohol were purchased from Aladdin. Diethyl ether, dodecyl-tetradecyl-dimethylamine, and sodium tungstate were purchased from Wilmar. The above reagents were analytically pure samples. The standard samples used for gas chromatography (1-dodecene, 1-octene, dodecane epoxide and epoxoctane) were chromatographically pure and purchased from Aladdin.

2.2 Synthesis of surfactant DDC

The chemical structure of *N*1,*N*3-didodecyl, tetradecyl-2-hydroxy-*N*1,*N*1,*N*3,*N*3-tetramethyl-1,3-propane-diaminium chloride (DDC) was depicted in Scheme 1, which was a type of mixture, with the 3 : 1 molar ratio of dodecylamine to tetradecylamine. The synthesis was conducted under oxygen-free conditions. Specifically, 2 mol of 1,3-dichloro-2-propanol were added into a reactor containing 0.4 mol of dodecyl, tetradecyl-

dimethylamine in 70 mL of propanol, with a total mass of 0.3 wt% sodium carbonate acting as the catalyst. The reaction mixture was then refluxed at 60 °C for a period of 4–6 hours. After the reaction, a white precipitate was obtained through vacuum distillation for solvent removal, followed by 3 times recrystallization using a solvent mixture of ethyl acetate and ethanol (20 : 1).

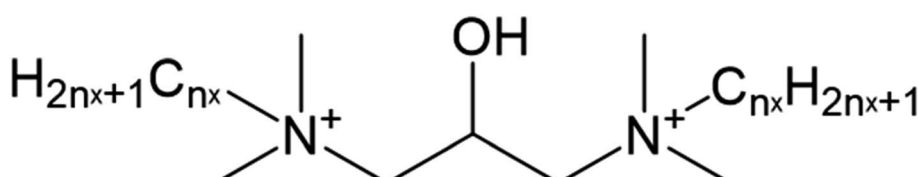
2.3 Synthesis of Wells-Dawson type phosphotungstic acid

Wells-Dawson phosphotungstic acid was synthesized by the documented method:³⁶ 50 g NaWO₄·2H₂O was dissolved in 60 mL distilled water, then poured 35.0 mL of concentrated phosphoric acid. The mixture was heated for 20 minutes until it turned milky white, then further heated to 120 °C for 8 hours. After the reaction, the mixture was cooled down to room temperature, and a specific quantity of concentrated hydrochloric acid was added to acidify the mixture. Diethyl ether was added to extract the phosphotungstic acid. Upon phase separation, the lower diethyl ether phase, consisted with diethyl ether, water and phosphotungstic acid were selected, and diethyl ether was evaporated under 40 °C conditions. The resulting residue was subjected to drying until a constant weight was achieved, yielding the final light yellow solid H₆P₂W₁₈O₆₂·14H₂O.

2.4 Catalyst preparation

1 mmol H₆P₂W₁₈O₆₂·14H₂O was dissolved in the 20 mL H₂O₂ (30wt%), and solution of 3 mmol of the surfactant DDC in 20 mL of anhydrous ethanol was also prepared. The anhydrous ethanol-DDC mixture was then added to the H₆P₂W₁₈O₆₂–H₂O₂ mixture and stirred for 1 hour. The resulting suspension was washed with anhydrous ethanol and repeated 3 or 4 times. Following filtration, the obtained precipitate was subjected to vacuum drying for a minimum of 12 hours, yielding the catalyst (P_W₁₈-DDC).

1 mmol H₃PW₁₂O₄₀·*x*H₂O was dissolved in the 20 mL H₂O₂ (30wt%), and solution of 3 mmol of the surfactant DDC in 20 mL of anhydrous ethanol was also prepared. The anhydrous ethanol-DDC mixture was then added to the H₃PW₁₂O₄₀–H₂O₂ mixture and stirred for 1 hour. The resulting suspension was washed with anhydrous ethanol and repeated 3 or 4 times. Following filtration, the obtained precipitate was subjected to vacuum drying for a minimum of 12 hours, yielding the catalyst (P_W₁₂-DDC).



Scheme 1 Structure of surfactant DDC, $n_1 = 12$, $n_2 = 14$.



2.5 Catalyst testing

2.5.1. Catalytic reaction. The selective oxidation of 1-dodecene was carried out in a four-neck round flask (250 mL) equipped with a mechanical agitator which provided a 250 rpm stirring rate and a reflux condenser.

0.1 mol 1-dodecene, 0.1 mol H_2O_2 (30% (mass) solution in water), and 5wt% catalysts were added into the flask, the mixture was heated by the heating jacket and stirred by a polytetrafluoroethylene stirring paddle, besides, a mercurial thermometer was immersed into the solution to make accurate temperature measurements. Due to the different reaction conditions of these 2 catalysts, the specific reaction conditions would be provided in results and discussion.

2.5.2. Gas chromatographic and calculation method. The concentration of α -olefin and epoxyalkane were analyzed by gas chromatography (GC-8860A, Agilent, the US) with a flame-ionization detector and a HP-5 column (35 m \times 0.32 mm, film: 0.5 mm). The temperature of the injector and detector was 300 °C, and 300 °C respectively. The initial temperature of column was 100 °C for 0 minutes, then raised column temperature at 10 °C per minute to 200 °C for 0 minutes, and 50 °C per minute to 320 °C for 5 minutes at the last. High-purity nitrogen was used as the carrier gas.

Analysis of reaction products were used by external standard method. The conversion of α -olefin and selectivity of epoxyalkane were calculated according to the formula below: Conversion $X = (C_0 - C_t)/C_0$, C_0 , C_t represents the initial concentration of the reactant and the concentration at time t respectively. Yield $\gamma = C_{pt}/C_{p0}$, C_{pt} , C_{p0} represent the concentration at time t and the theoretical concentration of the product respectively. Selectivity $S = \gamma/X$. The curves of standard samples were given in ESI (Fig. S1†).

2.5.3. Catalyst characterization. FT-IR analysis: Fourier transform infrared spectroscopy (FT-IR) was used on a VERTEX 70 spectrophotometer (Bruker, GRE) under a dry air condition at room temperature by the KBr pellets method. Scanning electron microscope (SEM) test was performed on TESCAN MIRA LMS. Elemental analysis was performed on Vario EL CUBE. ICP-MS test was performed on Agilent 5110(OES). X-ray photoelectron spectroscopy (XPS) was performed on Thermo Scientific K-Alpha, and the spectra were charge-corrected using a signal located at 284.5 eV. Small-angle X-ray scattering (SAXS) was performed on SAXSess mc2. UV-vis spectra were performed on Hitachi U4150. Powder XRD was performed on D8 ADVANCE A25. Raman spectra analysis were performed on Horiba LabRAM HR Evolution.

3. Results and discussion

3.1 Catalytic testing

3.1.1. Catalytic performance. Due to the solubility of PW₁₂-DDC under high temperature conditions without solvents, the catalytic performance of P₂W₁₈-DDC and PW₁₂-DDC in the epoxidation of 1-dodecene was evaluated under the following conditions: 343 K, 1×10^{-4} mol catalyst dosage, mechanical stirring at 250 rpm, and a 2:1 ratio of H_2O_2 to 1-dodecene,

dosage of substrate: 0.1 mol. As depicted in Table 1, after 6 hours reaction, P₂W₁₈-DDC exhibited higher selectivity towards dodecane epoxide but lower conversion of 1-dodecene compared to PW₁₂-DDC. In contrast to PW₁₂-DDC, almost all of the P₂W₁₈-DDC catalyst could be recovered after the reaction.

Subsequently, the catalytic performance of different olefins under identical conditions was investigated (Table S1†). P₂W₁₈-DDC exhibited higher selectivity towards epoxides and lower conversion to olefins, especially notable in the case of 1-tetradecene, which showed 93% selectivity to tetradecane epoxide and 36% conversion. In comparison with other catalysts,^{37,38} P₂W₁₈-DDC demonstrated superior selectivity in the epoxidation of long-chain olefins within a relatively short reaction time (only 6 hours), although with the lower olefin conversion. Additionally, a notable advantage of this catalyst was its ability to maintain high catalytic activity under solvent-free conditions and be readily reused through a straightforward filtration process by anhydrous ethanol, thus reducing production costs and aligning with the concept of green chemistry.

3.1.2. Optimization of reaction conditions. P₂W₁₈-DDC exhibited negligible catalytic activity at temperatures below 323 K. The addition of Wells-Dawson type phosphotungstic acid or surfactants individually into the system did not result in any catalytic activity.

Initially, the impact of temperature was examined under other invariant reaction conditions (Fig. 1a), with all reaction times kept six hours. As the temperature surpassed 323 K, the conversion of 1-dodecene exhibited a steady increase, while the selectivity of dodecane epoxide initially rose before subsequently declining. At 333 K, P₂W₁₈-DDC demonstrated an optimal selectivity of 92% towards dodecane epoxide. Moreover, the yield of epoxy dodecane continued to rise as the temperature elevated from 323 K to 353 K. Considering both selectivity and product yield, 343 K was selected as the most suitable temperature for the reaction.

Subsequently, the impact of hydrogen peroxide was examined under 343 K with other invariant reaction conditions. The initial ratio of H_2O_2 to 1-dodecene was varied from 1:1 to 4:1. As depicted in Fig. 1b, elevated volumes of hydrogen peroxide led to greater conversion of 1-dodecene but lower selectivity of dodecane epoxide. Notably, the selectivity of dodecane epoxide dropped below 90% when the ratio of hydrogen peroxide to 1-dodecene was 2:1. Consequently, an initial ratio of 2:1 for H_2O_2 and 1-dodecene was deemed the relatively suitable condition.

Next, the influence of catalyst dosage was investigated using four different dosage levels, while keeping other conditions constant. As illustrated in Fig. 1c, P₂W₁₈-DDC exhibited the lowest conversion of 1-dodecene, along with the highest

Table 1 The results of direct epoxidation of dodecene catalyzed by different catalyst

No.	Catalyst	Conversion/%	Selectivity/%	Catalyst state
1	PW ₁₂ -DDC	49	85	Partial soluble
2	P ₂ W ₁₈ -DDC	35	90	Insoluble



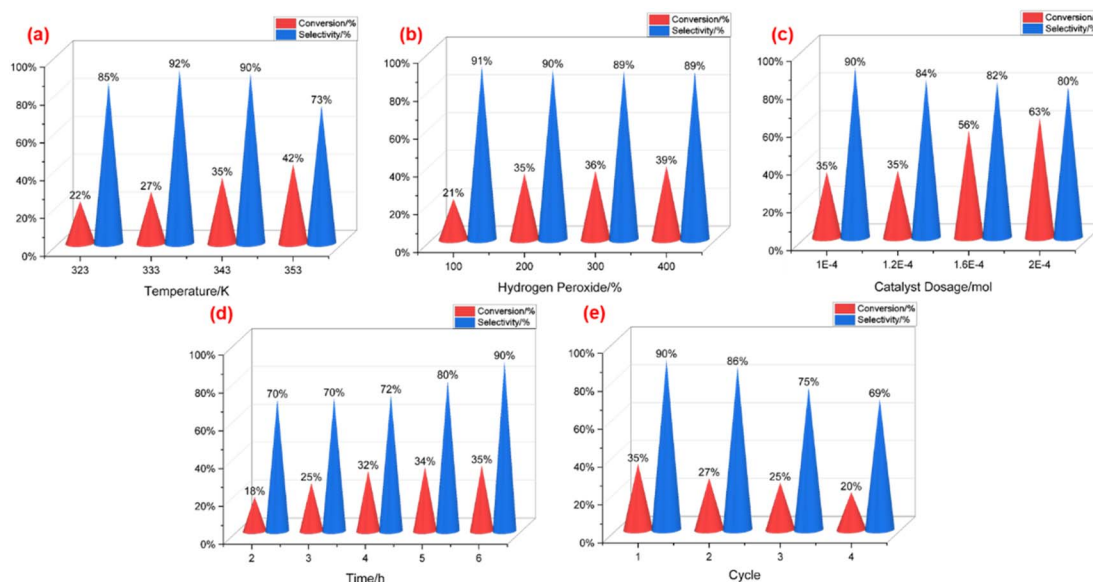


Fig. 1 (a) Effect of temperature. Catalyst dosage, 1×10^{-4} mol; 250 rpm; ratio of H_2O_2 and dodecane: 2 : 1, reaction time: 6 h; (b) effect of initial ratio of H_2O_2 and dodecane. Catalyst dosage, 1×10^{-4} mol; temperature, 343 K; 250 rpm, reaction time: 6 h; (c) effect of catalyst dosage. Temperature, 343 K; 250 rpm; ratio of H_2O_2 and dodecane: 2 : 1, reaction time: 6 h; (d) effect of reaction times. Catalyst dosage, 1×10^{-4} mol; temperature, 343 K; 250 rpm; ratio of H_2O_2 and dodecane: 2 : 1; (e) reuse of the catalyst. Catalyst dosage, 1×10^{-4} mol; 250 rpm; temperature, 343 K; ratio of H_2O_2 and dodecane: 2 : 1, reaction time: 6 h.

selectivity towards epoxy dodecane, at 1×10^{-4} mol catalyst dosage. With an increase in catalyst dosage, the interfacial tension between oil and water decreased due to the presence of long-chain quaternary ammonium salt. This facilitated the formation of smaller droplets and increased the interface area between water phase and oil phase, thereby enhancing the reaction rate. The conversion of 1-dodecene continued to rise, and the selectivity of epoxy dodecane decreased from 90% to 80% as the catalyst dosage increased from 1×10^{-4} mol to 2×10^{-4} mol. This trend indicated that an elevated amount of catalyst also resulted in the formation of by-products.

Under the determined appropriate conditions, the influence of reaction time was investigated for 2 to 6 hours. As depicted in Fig. 1d, the selectivity of epoxy dodecane exhibited a rapid increase as the reaction progressed, reaching its maximum at 6 hours, while the conversion of 1-dodecene increased at a slower rate.

Finally, cycle experiments were conducted under the specified conditions: Catalyst dosage at 1×10^{-4} mol; rotational speed at 250 rpm; temperature at 343 K; and an initial ratio of H_2O_2 to 1-dodecene at 2 : 1. The catalyst was subsequently filtered for recycling and washed with anhydrous ethanol at least three times after each reaction cycle. The outcomes were presented in Fig. 1e. As the P_2W_{18} -DDC catalyst was reused, the conversion of 1-dodecene experienced a gradual reduction, while the selectivity of epoxy dodecane dropped steeply after three cycles of recycling. These findings suggested that the catalyst possesses a limited recycling capacity.

3.2 Catalyst characterization

3.2.1. Morphology analysis. Small powder XRD was used to reveal the crystal structure of the catalyst. In Fig. 2, both catalysts exhibited amorphous structures, in the XRD pattern of PW_{12} -DDC, three different peaks were observed, which were 2 theta of 9.73, 19.2 and 25°, indicated the (110), (220), (222) crystal faces of $\text{H}_3\text{PW}_{12}\text{O}_{40}$ (JCPDS: #50-0304). Compared with $\text{H}_3\text{PW}_{12}\text{O}_{40}$ at 10.62, 20 and 26.7°, the addition of quaternary ammonium salt made the interplanar spacing became larger. P_2W_{18} -DDC displayed only three broad peaks at 15.4, 24.6 and 27.2°, which were consistent with the structure of

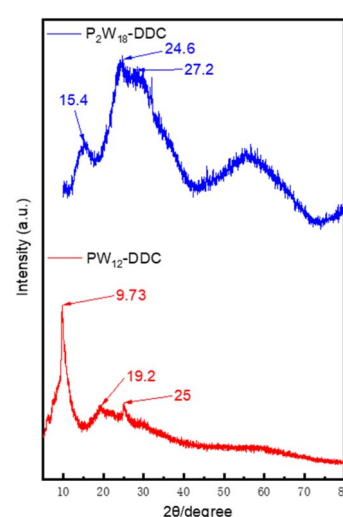


Fig. 2 XRD pattern of P_2W_{18} -DDC and PW_{12} -DDC.



$\text{H}_6\text{P}_2\text{W}_{18}\text{O}_{62}$.³⁶ Compared with $\text{P}_2\text{W}_{18}\text{-DDC}$, the crystal face of (110) in $\text{PW}_{12}\text{-DDC}$ still performed a strong diffraction, which could be attributed to the polarization of hydrogen bonding between quaternary ammonium salts and phosphotungstic acid. No obvious diffraction peaks of peroxy structure could be observed, which might be because that the crystal faces were covered by alkyl chains.^{39,40}

To further determine the microstructure of the catalyst, SAXS analysis was used to characterize $\text{P}_2\text{W}_{18}\text{-DDC}$ and $\text{PW}_{12}\text{-DDC}$. In the SAXS pattern presented in Fig. 3a, $\text{P}_2\text{W}_{18}\text{-DDC}$ exhibited two scattering peaks arising from ordered structures, characterized by q values of 0.190 nm^{-1} and 0.378 nm^{-1} , respectively. The nearly $1:2$ ratio of the q values was indicative of lamellar phases. Conversely, in the SAXS pattern of $\text{PW}_{12}\text{-DDC}$ (Fig. 3b), the q -value ratio was approximately $1:\sqrt{1.5}:\sqrt{4}$, indicating an irregular layered arrangement. The interlayer spacing (d -spacing) was determined from the q_1 value of the first scattering peak using the formula $d_1 = 2\pi/q_1$. For $\text{P}_2\text{W}_{18}\text{-DDC}$, the calculated d value was 3.3 nm , while for $\text{PW}_{12}\text{-DDC}$ it was 3.06 nm . This observation suggested that $\text{P}_2\text{W}_{18}\text{-DDC}$ possessed a greater layer spacing, which could be attributed to the larger peroxy structure of Wells–Dawson-type phosphotungstic acid. Furthermore, compared with the previously prepared catalysts,³⁵ quaternary ammonium salts with shorter chain lengths in $\text{PW}_{12}\text{-DDC}$ had performed longer interlayer spacing and more irregular lamellar phases, indicated that with the participation of hydrogen bonding, C–OH in DDC could combine a certain quantity of peroxy phosphotungstic acid, facilitated the binding of a certain quantity of peroxy phosphotungstic acid, resulting in the irregular arrangement between phosphotungstic acid molecules to form $\text{PW}_{12}\text{-DDC}$, while the larger peroxy structure of Wells–Dawson-type phosphotungstic acid could not

accommodate more phosphotungstic acid unit, made the hydrogen bonding ineffective. Due to the enhanced capacity of Wells–Dawson-type phosphotungstic acid to bind quaternary ammonium cations, scanning electron microscopy (SEM) was used to provide detailed micromorphological information. The micrographs of $\text{P}_2\text{W}_{18}\text{-DDC}$ and $\text{PW}_{12}\text{-DDC}$ were presented in Fig. S3 and S4,[†] respectively. The layered structures of both catalysts were observed, $\text{P}_2\text{W}_{18}\text{-DDC}$ demonstrated a more obvious and denser layered arrangement in comparison to $\text{PW}_{12}\text{-DDC}$.

3.2.2. Elemental analysis. In theory, 1 mol Wells–Dawson type phosphotungstic acid could theoretically combine with 3 mol surfactant, 1 mol Keggin type phosphotungstic acid could theoretically combine with 1.5 mol surfactant (Table S2[†]). To determine the relative content of quaternary ammonium salt and phosphotungstic acid of the catalyst, elemental analysis was performed. The elements of C, N, O, and H were conducted using an elemental analyzer, while analysis of P and W was carried out using ICP-MS. The results were presented in Table 2. The molar ratio of W to O in $\text{P}_2\text{W}_{18}\text{-DDC}$ was approximately $2:7$, and the molar ratio of P to O was nearly $2:39$. The molar ratio of P to W was $2:11$. Moreover, the molar ratio of P to N was nearly $4:9$, indicating that 1 mol Wells–Dawson type phosphotungstic acid molecule was capable of combining with a maximum of 2.25 mol surfactant DDC molecules. This suggested that the charges carried by Dawson type peroxy phosphotungstic acid was lower than the theoretical calculations. Furthermore, in theory, the molar ratio of W to P in $\text{PW}_{12}\text{-DDC}$ was $4:1$, N to P was nearly $3:1$, but in fact W to P in $\text{PW}_{12}\text{-DDC}$ was approximately $10:1$, N to P was nearly $8:1$, far greater than the ideal structure reported previously.³⁷ Although it is reported that the peroxy phosphotungstic acid anion would be converted to a more stable structure of $\text{PW}_{11}/\text{PW}_{12}$ during the immobilization process, more quaternary ammonium salts combined with Keggin type peroxy phosphotungstic acid in $\text{PW}_{12}\text{-DDC}$ might be attributed to the hydrogen bonding between peroxy phosphotungstic acid and surfactant DDC.

3.2.3. FT-IR analysis. FT-IR spectra were used to perform the chemical bonds in the catalyst. In the spectra presented in Fig. 4, both $\text{PW}_{12}\text{-DDC}$ and $\text{P}_2\text{W}_{18}\text{-DDC}$ exhibited peaks at 1470 cm^{-1} (C–N vibration), confirming the successful combination of the surfactant DDC with phosphotungstic acid. The $\text{PW}_{12}\text{-DDC}$ showed the characteristic peak at 1080 cm^{-1} (P–O), 980 cm^{-1} (W=O), 890 cm^{-1} (W–O_b–W), and 725 cm^{-1} (W–O_c–W), compared with the Keggin-type phosphotungstic acid at 1080 cm^{-1} (P–O), 980 cm^{-1} (W=O), 890 cm^{-1} (W–O_b–W), and 800 cm^{-1} (W–O_c–W), the peaks at 820 cm^{-1} was attributed to the –O–O–, while the peaks of W–O_c–W performed a red shift from 800 cm^{-1} to 725 cm^{-1} , which could not be observed at

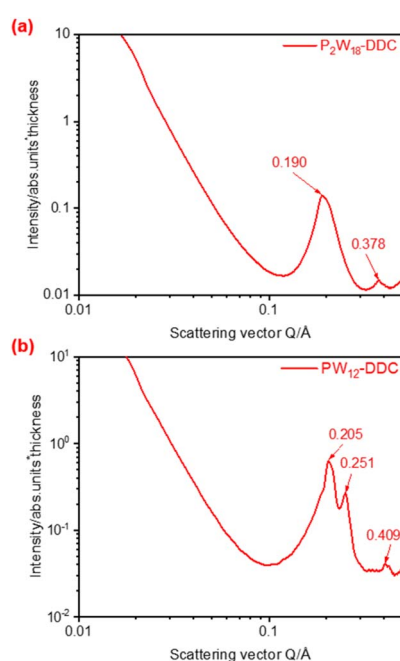


Fig. 3 (a) The SAXS pattern of $\text{P}_2\text{W}_{18}\text{-DDC}$, (b) The SAXS pattern of $\text{PW}_{12}\text{-DDC}$.

Table 2 The results of elemental analysis (mol%)

	C/%	H/%	O/%	N/%	P/%	W/%
$\text{P}_2\text{W}_{18}\text{-DDC}$	24.11	55.67	14.06	1.56	0.68	3.92
$\text{PW}_{12}\text{-DDC}$	25.88	58.94	11.45	1.59	0.19	1.95



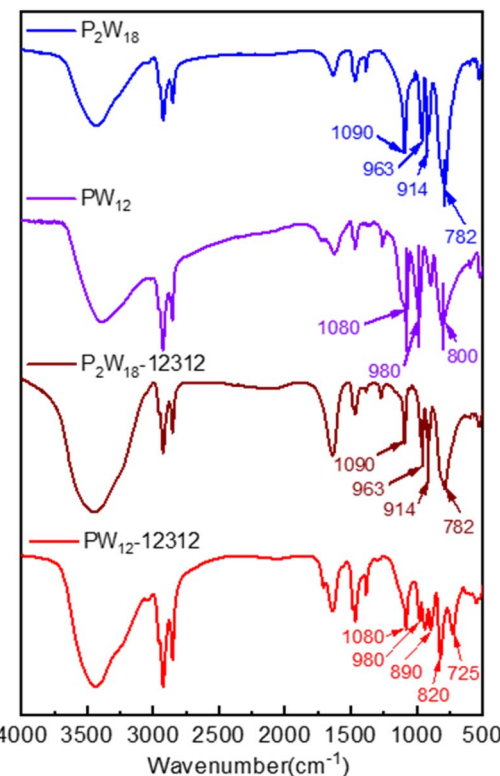


Fig. 4 FT-IR spectra of the $\text{H}_6\text{P}_2\text{W}_{18}\text{O}_{62}$, $\text{H}_3\text{O}_{40}\text{PW}_{12}$, P_2W_{18} -DDC and PW_{12} -DDC.

hydroxy-free quaternary ammonium salt and phosphotungstate acid system, leading to the formation of hydrogen bonding between C-OH and W-O_c-W, moreover, the new band at 938 cm⁻¹ originally branched from 980 cm⁻¹ for W=O was assignable to the reduced W⁵⁺ species due to the intramolecular charge transfer from quaternary ammonium salt to terminal oxygen of PW.⁴¹ Conversely, the peaks at 914, 963, and 1090 cm⁻¹ showed the successful synthesis of Wells-Dawson type of phosphotungstic acid, with the similar peaks in catalyst P_2W_{18} -DDC, they exhibited common corresponding to the vibration of W-Ob-W, W=O, and P-O, respectively. In conjunction with the elemental analysis results, treatment with H_2O_2 resulted in the conversion of partial $\text{H}_6\text{P}_2\text{W}_{18}\text{O}_{62}$ into a peroxy structure. No significant shift was observed in P_2W_{18} -DDC, indicating that the combination of Dawson type phosphotungstic acid and quaternary ammonium salts occurred solely through ionic bonding. Furthermore, both catalysts retained the characteristic peak of W-O_c-W, confirming the preservation of their Keggin and Wells-Dawson type phosphotungstic acid structures.

3.2.4. XPS analysis. The XPS spectra were used to reveal the elemental composition on the surface of catalysts. In the XPS spectra shown in Fig. 5a, the full spectra of P_2W_{18} -DDC exhibited obvious peaks at 531, 284, and 36 eV, corresponding to the O 1s, C 1s, and W 4f signals respectively. Similar peaks were observed for PW₁₂-DDC as shown in Fig. 5. Following the peaks separation method described by Zhao, *et al.*⁴² Fig. 5b revealed the fitting of the W element in the catalyst into five

distinct W 4f peaks. Specifically, the peak at 34 eV for W 4f_{5/2} were attributed to W⁴⁺, the peak at 34.9 eV for W 4f_{7/2} and 37 eV for W 4f_{5/2} were attributed to W⁵⁺, while the peaks at 35.8 eV for W 4f_{7/2} and 37.9 eV for W 4f_{5/2} were attributed to W⁶⁺. The surface elemental content of W⁵⁺ in P_2W_{18} -DDC was approximately 79.71%, with the elemental content of W⁴⁺ was 8.18%. In comparison with Wells-Dawson type phosphotungstic acid, a portion of W on the surface of P_2W_{18} -DDC was reduced to W⁵⁺, suggesting the disruption of the Wells-Dawson type phosphotungstic acid structure on the surface, which could combine with more negative charges, increase the interaction between surfactant and WO_x. But the W 4f signal in PW₁₂-DDC in Fig. 5e was divided into 4 peaks, the peak at 34 eV for W 4f_{5/2} and the peak 36.1 eV for W 4f_{7/2} were attributed to W⁴⁺, the peak at 34.9 eV for W 4f_{5/2} and the peak at 37 eV for W 4f_{7/2} were attributed to W⁵⁺, while the W⁶⁺ species were not observed.

In the O 1s spectra in Fig. 5c and f, the peak fitting revealed three distinct peaks, the peak at 529.5 eV was attributed to lattice oxygen, while the peak at 530.5 eV corresponded to highly oxidative oxygen species, the peak at 531.5 eV was attributed to surface oxygen species. The surface O in catalyst could be classified as reaction intermediates and other active O species, such as W(O)₂ and less C-OH of quaternary ammonium salt, while W=O could be attributed to highly oxidative O, which was reported to be closely correlated to surface O, could participate in the reaction by combining O to become an active substance, W-O-W could be attributed to lattice O.^{43,44} During the catalytic reaction, only surface oxygen, along with highly oxidative oxygen participate in the reaction process. It was worthy noting that although the relative content of quaternary ammonium salts in PW₁₂-DDC was relatively higher than P_2W_{18} -DDC, the content of surface O specie was just 9.36%, lower than 24.87% in P_2W_{18} -DDC, but the content of highly oxidative O specie and FWHM were higher than P_2W_{18} -DDC, which could be attributed to the formation of hydrogen bonding between phosphotungstic acid and surfactant DDC during the preparation of PW₁₂-DDC.

3.3 Mechanism analysis

3.3.1. SEM analysis after reaction. The utilized P_2W_{18} -DDC was further categorized into two groups: unwashed (Fig. S5†) and washed with anhydrous ethanol (Fig. S5†). Both exhibited distinct lamellar phases, underscoring the catalysts' insolubility in both oil and water phases. In Fig. S5,† it was evident that the majority of olefins and epoxides were deposited on the catalyst surface, while the Fig. S6† illustrated that a significant portion of 1-dodecene was effectively removed by anhydrous ethanol washing while maintaining the layered accumulation. The SEM picture of utilized PW₁₂-DDC was shown in Fig. S7,† although the layered structure could still be observed on the catalyst, the layered phase structure performed less distinct, which could be attributed to the further coverage of quaternary ammonium salts and the loss of phosphotungstic acid. To confirm this conclusion, relevant characterizations were analyzed in the following sections.



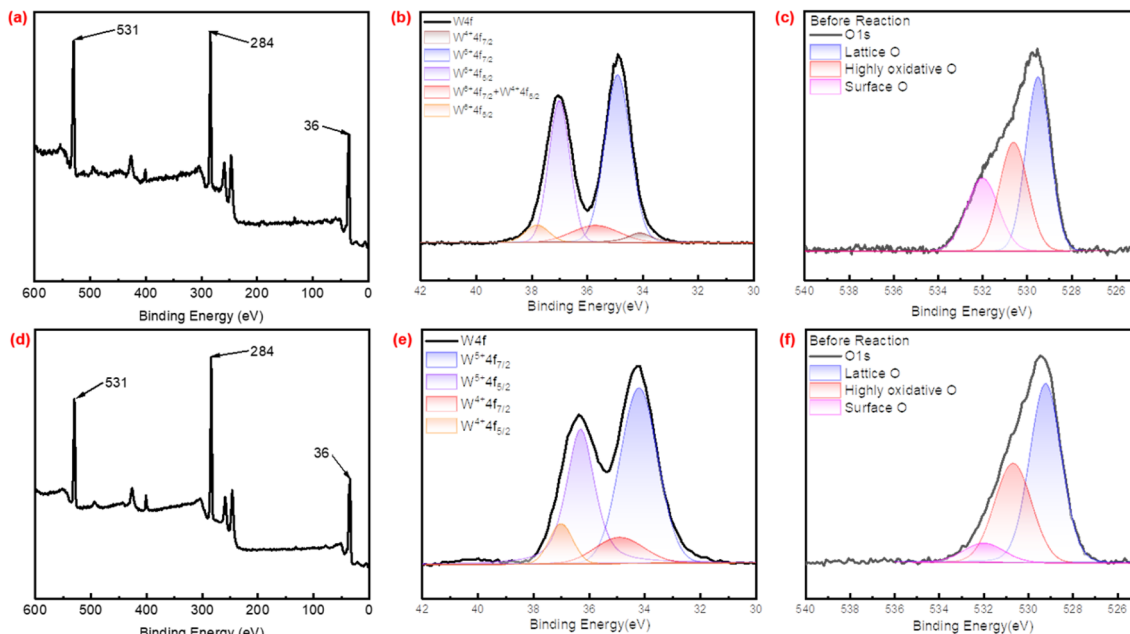


Fig. 5 (a) The full XPS spectra of the P_2W_{18} -DDC, (b) the W 4f XPS spectra of P_2W_{18} -DDC, (c) the O 1s XPS spectra of P_2W_{18} -DDC (d) the full XPS spectra of the PW_{12} -DDC, (e) the W 4f XPS spectra of PW_{12} -DDC, (f) the O 1s XPS spectra of PW_{12} -DDC.

3.3.2. FT-IR analysis after reaction. In the FT-IR spectra of the utilized P_2W_{18} -DDC (Fig. 6), the structural features remained largely unaltered after the reaction. The characteristic peaks at 914 , 963 , and 1090 cm^{-1} , attributed to the vibrations of $W-O_b-W$, $W=O$, and $P-O$, respectively, were still prominently present. Interestingly, in comparison to after reaction P_2W_{18} -DDC, the majority of the $W=O$ peaks and $-O-O-$ peaks in PW_{12} -DDC nearly vanished (at 980 cm^{-1} and 820 cm^{-1}), leaving only very faint residual peaks, the peak of $W-O_c-W$ at 725 cm^{-1} increased noticeably, which was not observed before.³⁵ The reason for these significant conversion among $W=O$, $W(O_2)$ and $W-O_c-W$ might not only be due to the transformation from $W=O$ to $W(O_2)$, the peroxidation from $W-O_c-W$ to $W(O_2)$ induced by hydrogen bonding also involved in the reaction

during the catalytic reaction. Furthermore, the peaks at 1080 cm^{-1} and 1107 cm^{-1} also confirmed the formation of hydrogen bonding among the terminal oxygen atoms of PW_{12} anions and the quaternary ammonium salt,⁴⁵ leading to the redox properties of W species tuned by $W-O\cdots H$.

3.3.3. XPS analysis after reaction. In the XPS spectra of C 1s in P_2W_{18} -DDC and PW_{12} -DDC before and after reaction (Fig. S8†), the C–N content of these two catalysts remained basically unchanged, proving that the use of anhydrous ethanol could effectively wash off residual olefins and epoxides from the catalyst surface.

The XPS spectra of O 1s and W 4f of utilized P_2W_{18} -DDC and PW_{12} -DDC were demonstrated in Fig. S9.† After reaction, the ratio of surface O (C–OH and $W(O_2)$) to lattice O ($W-O-W$) for the catalyst was lower than before the reaction in both catalysts. This reduction in ratio likely contributed to the decrease in catalytic reactivity of catalysts, but the content of highly oxidative O nearly unchanged, indicating the transformation between $W(O_2)$ and $W=O$. Notably, after the reaction, the content of W^{5+} in P_2W_{18} -DDC have been increased with the decreased content of W^{4+} (Fig. S9d†), with a narrower FWHM of W^{5+} peaks in 34.9 eV . This observation suggested that during the reaction, some of the W^{5+} and W^{4+} species were oxidized back to higher valence states. Conversely, in the W 4f spectra of PW_{12} -DDC (Fig. S9b†), the surface tungsten (W) species of PW_{12} -DDC predominantly existed in the +5 valence state or lower. After the reaction, a decrease in W^{5+} contents have been observed, while the content of highly oxidative O and lattice O increased obviously, indicating the formation of WO_x groups instead of the original structure of phosphotungstic acid,⁴⁴ leading to the weakening of layered structure observed on the SEM image.

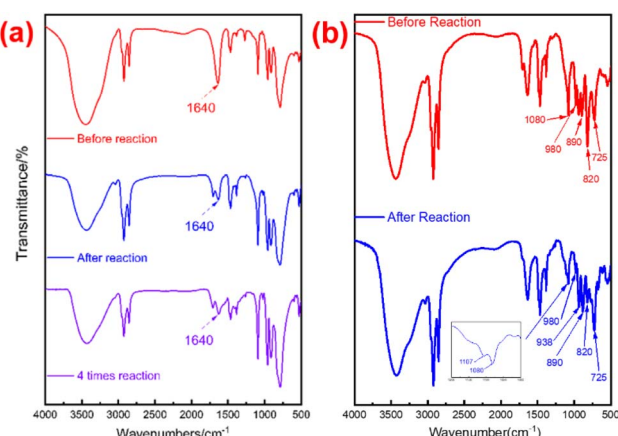


Fig. 6 (a) FT-IR spectra of P_2W_{18} -DDC, (b) FT-IR spectra of PW_{12} -DDC.



3.3.4. UV-vis analysis after reaction. The UV-visible spectra of P_2W_{18} -DDC are presented in Fig. S10.† Notably, a region of higher energy, ranging from 210 to 230 nm, was observed in Fig. S10a,† which could be attributed to charge transfer between the metal and oxygen species, as also indicated at 238 nm in Fig. S10b.†⁴⁵ After the reaction of P_2W_{18} -DDC (Fig. S10a†), it is noteworthy that the peak at 300 nm experienced a blue shift to 290 nm. Additionally, the absorption edge extended from approximately 480 nm to 430 nm, indicating the oxidation of the metal center to a relatively higher valence state, conversely, the absorption edge of PW_{12} -DDC experienced a subtle red shift, indicating the transfer to a lower valence state of the metal center, which was consistent with the results of XPS analysis.

3.3.5. Raman spectra analysis. The Raman spectra of utilized P_2W_{18} -DDC and PW_{12} -DDC were also performed. As depicted in Fig. 7, after reaction, the disappearance of the peaks at 110 cm^{-1} (structure of Wells–Dawson type phosphotungstic acid) and 620 cm^{-1} (vibration of C–O) indicated the formation of more peroxy structure in P_2W_{18} -DDC. However, the PW_{12} -DDC showed noticeable change after reaction (Fig. 8). Firstly, compared with Keggin type phosphotungstic acid (Fig. S11†), the tungsten correlation peaks at 195, 312 and 552 cm^{-1} in PW_{12} -DDC showed a red shift, which could be contributed the hydrogen bonding between W–O–W and C–OH,⁴⁶ while P_2W_{18} -DDC showed a blue shift, indicating the larger groups of peroxy structure in P_2W_{18} -DDC, making the influence of hydrogen bonding ineffective. It could be observed the peaks at 1445 cm^{-1} and 2900 cm^{-1} intensified, leading to the removal of phosphotungstic acid structure. The peaks at 880 and 952 cm^{-1} have performed a red shift to 895 and 970 cm^{-1} , indicating the transformation from $W(O_2)$ to $W=O$,⁴⁷ the blue shift from 552

to 530 cm^{-1} revealed the transform between $W-O_c-W$ and $W(O_2)$, while the red shift from 195 to 232 cm^{-1} , 312 to 331 cm^{-1} could also confirm this conversion. Furthermore, compared with P_2W_{18} -DDC, two new peaks at 100 cm^{-1} and 998 cm^{-1} were observed in the PW_{12} -DDC, indicated that during the catalytic reaction, the peroxy structure of catalyst underwent a process of forming WO_x groups influenced by hydrogen bonding between DDC and phosphotungstic acid,⁴³ while the P_2W_{18} -DDC tended to form the peroxy structure. Combined with the results of FT-IR, XPS spectra and Raman spectra, after the reaction, a portion of the $W-O-W/W=O$ species involved in the reaction might not return to their original structure, but rather combine with the remaining C–OH in quaternary ammonium salts through hydrogen bonding to form groups like $WO_{3/4}$.

3.3.6. Possible reaction route. In summary, there exist two distinct catalytic reaction pathways in these catalysts, which was shown in Fig. 9. In the epoxidation reaction catalyzed $W-O-W$ species, due to the hydrogen bonds combined with $W-O-W$ and C–OH, the electrophilicity of $W-O-W$ species were enhanced by hydrogen bonding,^{48,49} a portion of $W-O-W$ could combine with oxygen to form $W(O_2)$, then those peroxy structure and $W(O_2)$ formed from $W=O$ (phosphotungstic acid) participates in the catalytic reaction. After the reaction, the $W(O_2)$ species transform into $W-O-W$ to next catalytic reaction. Conversely, in the epoxidation reaction catalyzed by $W=O$ species, the reaction pathways were the same as previous study,³⁷ the $W=O$ species combine with oxygen to form $W(O_2)$. After the reaction, a portion of the $W(O_2)$ species revert to $W=O$, while the remaining $W(O_2)$ species retain their hypervalent state structure. By using various characterization methods, it is proved

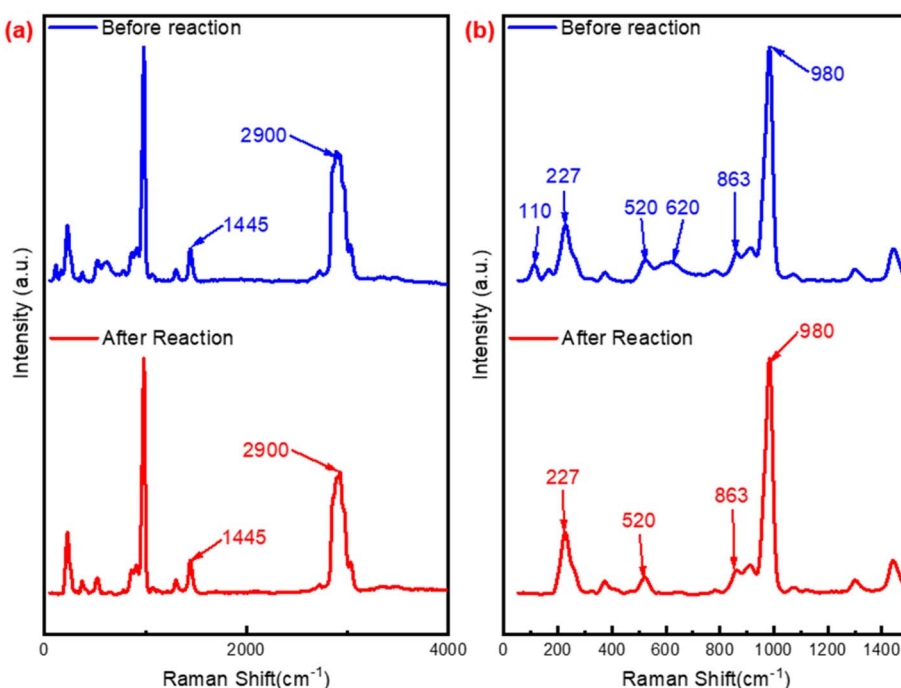


Fig. 7 Raman spectra of P_2W_{18} -DDC and used P_2W_{18} -DDC (a) range from 50 to 4000 cm^{-1} ; (b) range from 50 to 1500 cm^{-1} .



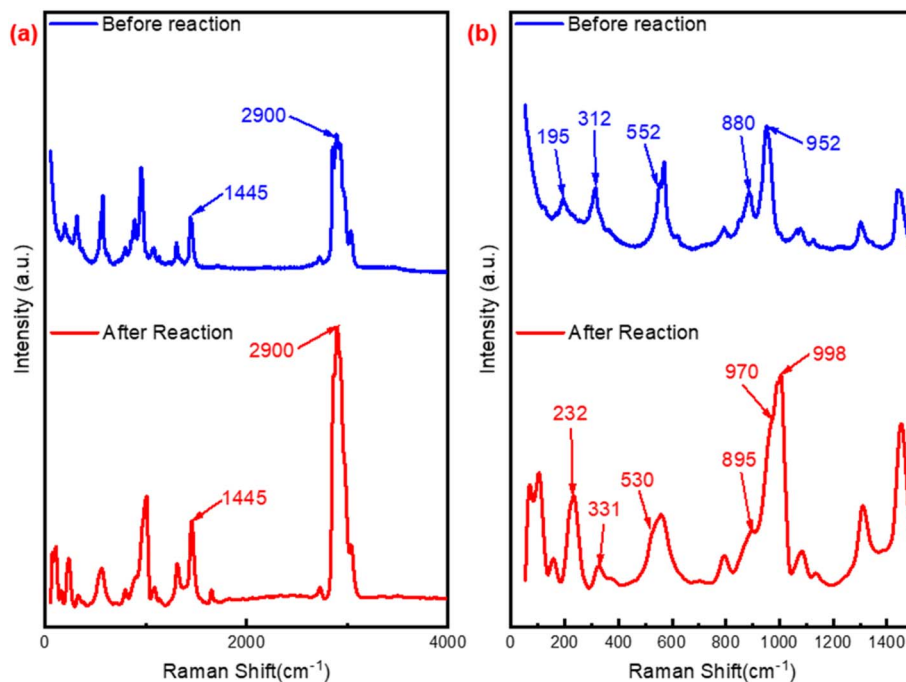


Fig. 8 Raman spectra of PW₁₂-DDC and used PW₁₂-DDC (a) range from 50 to 4000 cm⁻¹; (b) range from 50 to 1500 cm⁻¹.

that the catalyst prepared by Keggin type phosphotungstic acid would work through the above two routes in the catalytic reaction. While there was only one route (W(O₂) formed from W=O) worked in catalytic reaction of the catalyst prepared by Wells-Dawson type phosphotungstic acid.

4. Conclusions

In this study, two new types of catalyst was prepared to utilize Wells-Dawson-type phosphotungstic acid and Keggin type phosphotungstic acid combined with a biquaternary ammonium cation. Various characterizations were used to elucidate the fundamental structure of the catalysts. Compared with a catalyst synthesized with Keggin-type phosphotungstic acid, the Wells-Dawson-type phosphotungstic acid catalyst exhibited superior selectivity and recyclability, but lower conversion in the epoxidation of 1-dodecene. Subsequently, the impact of various

reaction conditions on catalyst performance was investigated, leading to the determination of optimal reaction conditions under solvent-free circumstances, thereby highlighting its potential industrial applicability. Throughout the course of the reaction, significant structural alterations in the catalyst were observed. Consequently, a comparative analysis was conducted between the pre- and after-reaction states, enabling the deduction of the catalytic mechanism influenced by hydrogen bonds for the catalyst synthesized with Keggin type phosphotungstic acid. Notably, this mechanism revealed a distinct reaction pathway in contrast to catalysts synthesized with Wells-Dawson type phosphotungstic acid.

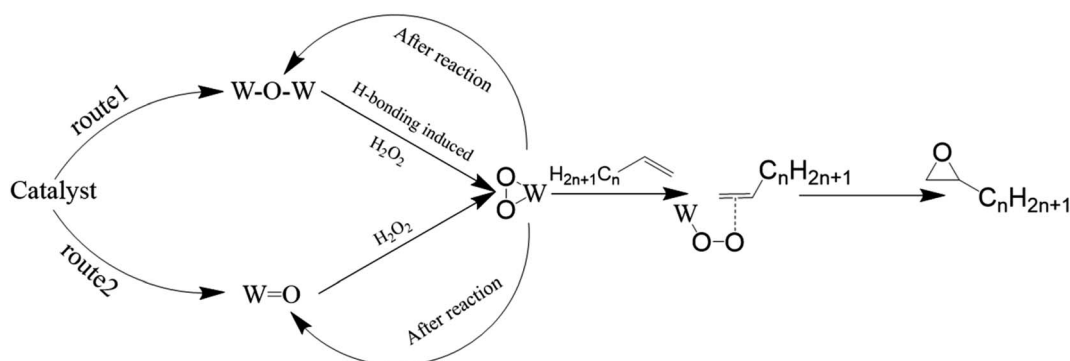


Fig. 9 Reaction route of catalysts.



Conflicts of interest

The authors declare that they have no known competing financial interests or personal relationships that could have appeared to influence the work reported in this paper.

Acknowledgements

This work was supported by the Basic research project of POLY sinolight (ZQ2021JC01) and the Project of JALA Research Funds (JALA2021).

References

- 1 J. Liu, G. Yang, Y. Liu, Z. Zhou, Z. Zhang and X. Hu, Selective Oxidation of Cyclohexene with H_2O_2 Catalyzed by Resin Supported Peroxo Phosphotungstic Acid Under Mild Conditions, *Catal. Lett.*, 2021, **151**, 147–152.
- 2 J. W. Bae and K.-Y. Lee, Special issue of the 15th Korea–Japan Symposium on Catalysis (15th KJSC), *Res. Chem. Intermed.*, 2016, **42**, 1–2.
- 3 B. Bahramian, V. Mirkhani, M. Moghadam and S. Tangestaninejad, Selective alkene epoxidation and alkane hydroxylation with sodium periodate catalyzed by cationic Mn(III)-salen supported on Dowex MSC1, *Appl. Catal., A*, 2006, **301**, 169–175.
- 4 M. A. Nasser, A. Allahresani and H. Raissi, Grafting of a chiral Mn(III) complex on graphene oxide nanosheets and its catalytic activity for alkene epoxidation, *RSC Adv.*, 2014, **4**, 26087–26093.
- 5 Y.-L. Hu, Y.-W. Liu and D.-J. Li, Efficient and convenient epoxidation of alkenes to epoxides with H_2O_2 catalyzed by $Co(OAc)_2$ in ionic liquid $[C_{12}Py][PF_6]$, *J. Iran. Chem. Soc.*, 2015, **12**, 2179–2184.
- 6 A. Bafti, M. Razum, E. Topić, D. Agustin, J. Pisk and V. Vrdoljak, Implication of oxidant activation on olefin epoxidation catalysed by Molybdenum catalysts with aroylhydrazone ligands: Experimental and theoretical studies, *Mol. Catal.*, 2021, **512**, 111764.
- 7 M. Jafarpour, H. Kargar and A. Rezaeifard, A synergistic effect of a cobalt Schiff base complex and TiO_2 nanoparticles on aerobic olefin epoxidation, *RSC Adv.*, 2016, **6**, 79085–79089.
- 8 R. Dileep and B. J. Rudresha, An ionic liquid immobilized copper complex for catalytic epoxidation, *RSC Adv.*, 2015, **5**, 65870–65873.
- 9 A. Freites Aguilera, J. Rahkila, J. Hemming, M. Nurmi, G. Torres, T. Razat, P. Tolvanen, K. Eränen, S. Leveneur and T. Salmi, Epoxidation of Tall Oil Catalyzed by an Ion Exchange Resin under Conventional Heating and Microwave Irradiation, *Ind. Eng. Chem. Res.*, 2020, **59**, 10397–10406.
- 10 J. Rakhtshah, A comprehensive review on the synthesis, characterization, and catalytic application of transition-metal Schiff-base complexes immobilized on magnetic Fe_3O_4 nanoparticles, *Coord. Chem. Rev.*, 2022, **467**, 214614.
- 11 M. Mitra, O. Cusso, S. S. Bhat, M. Sun, M. Cianfanelli, M. Costas and E. Nordlander, Highly enantioselective epoxidation of olefins by H_2O_2 catalyzed by a non-heme Fe(ii) catalyst of a chiral tetradentate ligand, *Dalton Trans.*, 2019, **48**, 6123–6131.
- 12 X.-Y. Shi, P.-M. Wang, K.-Y. Liu, X.-F. Dong, X.-Y. Han and J.-F. Wei, Peroxophosphotungstate held in an ionic liquid brush: an efficient and reusable catalyst for the dihydroxylation of olefins with H_2O_2 in neat water, *Appl. Organomet. Chem.*, 2014, **28**, 760–763.
- 13 Y. Li, S. Pan, R. Han, J. Gao, D. Liu and J. Gui, Rational Design of Phosphotungstate Hybrids with Dual Active Sites for Efficient Catalytic Oxidation, *Catal. Lett.*, 2023, **153**, 3092–3102.
- 14 V. Jallet, G. Guillemot, J. Lai, P. Bauduin, V. Nardello-Rataj and A. Proust, Covalent amphiphilic polyoxometalates for the design of biphasic microemulsion systems, *Chem. Commun.*, 2014, **50**, 6610–6612.
- 15 F. Zhang, Y. Dong, S. Lin, X. Gui and J. Hu, A novel amphiphilic phase transfer catalyst for the green epoxidation of soybean oil with hydrogen peroxide, *Mol. Catal.*, 2023, **547**, 113384.
- 16 P. Mekrattanachai, C. Cao, Z. Li, H. Li and W. Song, Cobalt immobilized on hydroxyapatite as a low-cost and highly effective heterogeneous catalyst for alkenes epoxidation under mild conditions, *RSC Adv.*, 2018, **8**, 37303–37306.
- 17 J. Tong, W. Wang, L. Su, Q. Li, F. Liu, W. Ma, Z. Lei and L. Bo, Highly selective oxidation of cyclohexene to 2-cyclohexene-1-one over polyoxometalate/metal–organic framework hybrids with greatly improved performances, *Catal. Sci. Technol.*, 2017, **7**, 222–230.
- 18 C. Venturello, E. Alneri and M. Ricci, A new, effective catalytic system for epoxidation of olefins by hydrogen peroxide under phase-transfer conditions, *J. Org. Chem.*, 1983, **48**, 3831–3833.
- 19 M.-L. Wang and T.-H. Huang, Kinetic Study of the Epoxidation of 1,7-Octadiene under Phase-Transfer-Catalysis Conditions, *Ind. Eng. Chem. Res.*, 2004, **43**, 675–681.
- 20 Y. Ishii, K. Yamawaki, T. Ura, H. Yamada, T. Yoshida and M. Ogawa, Hydrogen peroxide oxidation catalyzed by heteropoly acids combined with cetylpyridinium chloride. Epoxidation of olefins and allylic alcohols, ketonization of alcohols and diols, and oxidative cleavage of 1,2-diols and olefins, *J. Org. Chem.*, 1988, **53**, 3587–3593.
- 21 A. Patel and R. Sadasivan, Hybrid Catalyst Based on Cu Substituted Phosphotungstate and Imidazole: Synthesis, Spectroscopic Characterization, Solvent Free Oxidation of Styrene with TBHP and Kinetics, *Catal. Lett.*, 2020, **150**, 353–364.
- 22 R. Sadasivan and A. Patel, Flexible oxidation of styrene using TBHP over zirconia supported mono-copper substituted phosphotungstate, *RSC Adv.*, 2019, **9**, 27755–27767.
- 23 U. Jameel, M. Zhu, X. Chen, Y. Liu and Z. Tong, Green epoxidation of cyclooctene with molecular oxygen over an ecofriendly heterogeneous polyoxometalate-gold catalyst $Au/BW_{11}/Al_2O_3$, *J. Zhejiang Univ., Sci. A*, 2016, **17**, 1000–1012.



24 F. Chen, X. Li, B. Wang, T. Xu, S.-L. Chen, P. Liu and C. Hu, Mechanism of the Cycloaddition of Carbon Dioxide and Epoxides Catalyzed by Cobalt-Substituted 12-Tungstenphosphate, *Chem.-Eur. J.*, 2012, **18**, 9870–9876.

25 X. Zuwei, Z. Ning, S. Yu and L. Kunlan, Reaction-Controlled Phase-Transfer Catalysis for Propylene Epoxidation to Propylene Oxide, *Science*, 2001, **292**, 1139–1141.

26 H. Gao, J. Yu, J. Du, H. Niu, J. Wang, X. Song, W. Zhang and M. Jia, Supramolecular Assembly Based on Octamolybdate and Triazole Derivative: Crystal Structure and Catalytic Application in Olefin Epoxidation, *J. Cluster Sci.*, 2014, **25**, 1263–1272.

27 Y.-F. Song and R. Tsunashima, Recent advances on polyoxometalate-based molecular and composite materials, *Chem. Soc. Rev.*, 2012, **41**, 7384–7402.

28 X. Sun, J. Zhang, X. Yuan and Z. Fu, A silicotungstate-based copper–viologen hybrid photocatalytic compound for efficient degradation of organic dyes under visible light, *CrystEngComm*, 2019, **21**, 5563–5567.

29 P. Zhang, T. Wang, H. Ma, R. Ma, Z. Xia, Q. Yang, X. Yang, G. Xie and S. Chen, Heterointerface Connection with Multiple Hydrogen-Bonding in Z-Scheme Heterojunction $\text{SiW}_9\text{Co}_3@\text{UiO-67-NH}_2$ Deciding High Stability and Photocatalytic CO_2 Reduction Performance, *Inorg. Chem.*, 2023, **62**, 20401–20411.

30 S.-M. Wang, Y.-H. Jin, L. Zhou, K.-H. Wang, H. J. Kim, L. Liu, E. Kim and Z. Han, Hydrogen-Bonded Organic Framework-Polyoxometalate-Based System for Electrochromic Devices, *ACS Appl. Mater. Interfaces*, 2023, **15**, 56242–56252.

31 X. Ma, S. Li, J. Hua, P. Ma, J. Wang and J. Niu, Designing a new organic–inorganic arsenomolybdate by modification of traditional Keggin-type building fragment, *J. Coord. Chem.*, 2013, **66**, 725–736.

32 S.-F. Jia, X.-L. Hao, Y.-Z. Wen and Y. Zhang, Synthesis, cytotoxicity, apoptosis and cell cycle arrest of a monoruthenium(II)-substituted Dawson polyoxotungstate, *J. Coord. Chem.*, 2019, **72**, 633–644.

33 T. Ma, J. Ding, R. Shao, W. Xu and Z. Yun, Dehydration of glycerol to acrolein over Wells–Dawson and Keggin type phosphotungstic acids supported on MCM-41 catalysts, *Chem. Eng. J.*, 2017, **316**, 797–806.

34 L. E. Briand, G. T. Baronetti and H. J. Thomas, The state of the art on Wells–Dawson heteropoly-compounds: A review of their properties and applications, *Appl. Catal., A*, 2003, **256**, 37–50.

35 L.-Z. Zhang, H.-B. Ju, T. Geng, D.-B. Li, Y.-J. Jiang and Y.-K. Wang, Study on the epoxidation of chain olefins using biquaternary ammonium phosphotungstic acid phase transfer catalysts under no-solvent condition, *Chem.-Eur. J.*, 2024, **30**, e202303559.

36 L. E. Briand, G. M. Valle and H. J. Thomas, Stability of the phospho-molybdcic Dawson-type ion $\text{P}_2\text{Mo}_{18}\text{O}_{62}^{6-}$ in aqueous media, *J. Mater. Chem.*, 2002, **12**, 299–304.

37 Z. Zhang, Q. Zha, Y. Liu, Z. Zhang, J. Liu and Z. Zhou, Study on the epoxidation of olefins with H_2O_2 catalyzed by biquaternary ammonium phosphotungstic acid, *Chin. J. Chem. Eng.*, 2023, **58**, 146–154.

38 S. Zhao, Y. Jia and Y.-F. Song, Highly efficient and selective oxidation of various substrates under mild conditions using a lanthanum-containing polyoxometalate as catalyst, *Appl. Catal., A*, 2013, **453**, 188–194.

39 Y. Wang, W. Li and L. Wu, Organic–Inorganic Hybrid Supramolecular Gels of Surfactant-Encapsulated Polyoxometalates, *Langmuir*, 2009, **25**, 13194–13200.

40 Y. Shen, X.-H. Lu, C.-C. Wei, X.-T. Ma, C. Peng, J. He, D. Zhou and Q.-H. Xia, Highly selective mono-epoxidation of dicyclopentadiene with aqueous H_2O_2 over heterogeneous peroxy-phosphotungstic catalysts, *Mol. Catal.*, 2017, **433**, 185–192.

41 M. Zhang, P. Zhao, Y. Leng, G. Chen, J. Wang and J. Huang, Schiff Base Structured Acid–Base Cooperative Dual Sites in an Ionic Solid Catalyst Lead to Efficient Heterogeneous Knoevenagel Condensations, *Chem.-Eur. J.*, 2012, **18**, 12773–12782.

42 J. Zhao, B. Hou, H. Guo, L. Jia, P. Niu, C. Chen, H. Xi, D. Li and J. Zhang, Insight into the Influence of WO_x -Support Interaction over Pt/W/SiZr Catalysts on 1,3-Propanediol Synthesis from Glycerol, *ChemCatChem*, 2022, **14**, e202200341.

43 Y. Wang, Z. Li, Z. Liu and X. Shi, Heterogenous carboxyl-functionalized bilayer ionic liquids/polyoxometalate catalysts for extractant-free oxidative desulfurization, *J. Mol. Liq.*, 2023, **373**, 121245.

44 H. Chen, C. Lim, M. Zhou, Z. He, X. Sun, X. Li, Y. Ye, T. Tan, H. Zhang, C. Yang, J. W. Han and Y. Chen, Activating Lattice Oxygen in Perovskite Oxide by B-Site Cation Doping for Modulated Stability and Activity at Elevated Temperatures, *Adv. Sci.*, 2021, **8**, 2102713.

45 Y. Chen, R. Tan, W. Zheng, Y. Zhang, G. Zhao and D. Yin, Dendritic phosphotungstate hybrids efficiently catalyze the selective oxidation of alcohols with H_2O_2 , *Catal. Sci. Technol.*, 2014, **4**, 4084–4092.

46 Y. Zhang, G. Ji and A. Li, Production of limonene epoxides from tire pyrolysis oil by polyoxometalate immobilized on SBA-15, *Process Saf. Environ. Prot.*, 2023, **178**, 287–295.

47 M. A. Rezvani and O. F. Miri, Synthesis and characterization of $\text{PbMn}/\text{NiO}/\text{PAN}$ nanosphere composite with superior catalytic activity for oxidative desulfurization of real fuel, *Chem. Eng. J.*, 2019, **369**, 775–783.

48 X. Lu, W.-J. Zhou, Y. Guan, A. Liebens and P. Wu, Enhancing ethylene epoxidation of a MWW-type titanosilicate/ H_2O_2 catalytic system by fluorine implanting, *Catal. Sci. Technol.*, 2017, **7**, 2624–2631.

49 M. Rocha, S. L. H. Rebelo and C. Freire, Enantioselective arene epoxidation under mild conditions by Jacobsen catalyst: The role of protic solvent and co-catalyst in the activation of hydrogen peroxide, *Appl. Catal., A*, 2013, **460–461**, 116–123.

